bioRxiv preprint doi: https://doi.org/10.1101/057620; this version posted June 7, 2016. The copyright holder for this preprint (which was not certified by peer review) is the author/funder, who has granted bioRxiv a license to display the preprint in perpetuity. It is made available under aCC-BY-NC-ND 4.0 International license.

# Functional brain segmentation using inter-subject correlation in fMRI

Jukka-Pekka Kauppi[†a,b,*], Juha Pajula[†c,*], Jari Niemi[c], Riitta Hari[d], Jussi Tohka[e,f,*]

[a] *University of Jyväskylä, Department of Mathematical Information Technology, Finland*
[b] *University of Helsinki, Department of Computer Science and HIIT, Finland*
[c] *Department of Signal Processing, Tampere University of Technology, Finland*
[d] *Department of Art, Aalto University, Helsinki, Finland*
[e] *Department of Bioengineering and Aerospace Engineering, Universidad Carlos III de Madrid, Leganes, Spain*
[f] *Instituto de Investigación Sanitaria Gregorio Marañon, Madrid, Spain*

**Abstract**

For a long time, neuroscientists have studied the human brain functions under an assumption that brain mechanisms are similar across a group of subjects under study. In real life, however, individuals process information more or less differently. To facilitate understanding of complex, natural processing of the brain, we present an exploratory data analysis approach called functional segmentation inter-subject correlation analysis (FuSeISC). The method provides a new type of functional segmentation of the brain characterizing not only brain areas with similar processing across subjects but also areas in which processing across subjects is different. We tested FuSeISC using functional magnetic resonance imaging (fMRI) data sets collected during traditional block-design stimuli (37 subjects) as well as naturalistic auditory narrative stimuli (19 subjects). The method identified spatially coherent clusters in various cortical areas with neuroscientifically plausible interpretations. Our results suggest FuSeISC as an interesting approach for exploratory analysis of human brain fMRI.

*Keywords:* functional magnetic resonance imaging, functional segmentation, inter-subject correlation, inter-subject variability, naturalistic stimulation, Gaussian mixture model, shared nearest neighbor graph

*Corresponding author. †Authors contributed equally to this work.

bioRxiv preprint doi: https://doi.org/10.1101/057620; this version posted June 7, 2016. The copyright holder for this preprint (which was not certified by peer review) is the author/funder, who has granted bioRxiv a license to display the preprint in perpetuity. It is made available under aCC-BY-NC-ND 4.0 International license.

## 1. Introduction

Traditionally, neuroimaging studies have utilized highly controlled experimental stimuli to study human brain functions. While these studies have been useful in providing answers for certain key functions of the brain, these studies do not resemble natural processing of the brain in daily life situations, where the brain continuously processes massive amounts of rich input information collected through different senses. In recent years, there has been a paradigm shift in neuroscience to conduct more naturalistic experiments better mimicking daily life situations to better understand complex processes of the brain.

While the amount of complex neuroimaging data sets collected in naturalistic experiments is increasing, a major bottleneck in these studies is the lack of proper analysis methods. So far, one of the most promising approaches to analyze complex functional magnetic resonance imaging (fMRI) data sets collected under naturalistic experiments has been so called *inter-subject correlation (ISC) analysis* [1]. ISC analysis has been used in many fMRI studies using naturalistic stimuli, such as movies/video [1, 2, 3, 4] and music [5, 6]. ISC-based analysis approach is conceptually simple, involving voxel-wise computation of correlation coefficients between time series of all subjects. Once the correlation coefficients have been computed across all participants exposed to an identical time-varying stimulus sequence, subject-pairwise correlation coefficients for each voxel can be averaged and subsequently thresholded to obtain brain maps indicating which regions exhibit ISC during the stimulus [7, 8]. A major strength of the ISC-based analysis is that the method can detect activated brain areas without modeling the expected hemodynamic response elicited by the stimuli [9].

Despite its benefits, the current ISC-based analysis techniques have several limitations. For example, similarly to model-based brain-mapping methods, such as those based on a general linear model (GLM; [10]), a conventional ISC-based mapping assumes that brain mechanisms are similar across subjects. In

bioRxiv preprint doi: https://doi.org/10.1101/057620; this version posted June 7, 2016. The copyright holder for this preprint (which was not certified by peer review) is the author/funder, who has granted bioRxiv a license to display the preprint in perpetuity. It is made available under aCC-BY-NC-ND 4.0 International license.

real life, however, individuals process identical sensory information more or less differently. It is likely that processes supporting higher-order brain functions are more variable than certain mechanisms of low-level sensory processing [11]. Therefore, a conventional ISC approach based on the averaging of correlation coefficients across all pairs of subjects finds high ISC values in sensory projection areas but may completely lose ISC in higher-order brain areas due to high inter-subject variability [12]. Such areas may contain active processing in different individuals, but these areas remain undetected due to averaging.

To better understand brain functions in areas where processing across subjects is variable (and average ISC may be low), improved analysis methods are needed. To this end, we propose analyzing the extent of variation in ISCs in addition to average ISCs: high variation in subject-pairwise correlation values is interesting because it suggests that some subjects share similar brain activity (high correlation) whereas some subjects do not (low or negative correlation). Instead, low variation in ISCs in the areas of low average ISC probably reflects noise since all subject-pairwise correlation values are close to zero in this case. This interpretation of ISC-based variability differs from traditional interpretation of variability in neuroimaging studies, where inter-subject variation is considered as noise. However, recent studies suggest that individual variability provides meaningful information that can help understanding complex processes and development of the brain [13, 14, 15, 16].

Another limitation of the conventional ISC approach is that it is *univariate*, meaning that it provides only voxel-wise information about the extent of the ISCs during a single fMRI time series. *Multivariate* methods, which are capable of integrating information across multiple voxels and consider several fMRI time series acquired during distinct stimuli, thus dividing the brain into functionally distinct segments[1], would be highly useful to provide additional insights into the spatial organization of the ISC.

We propose a multivariate approach to analyze the extent and variability of

[1] We use terms "cluster" and "functional segment" interchangeably.

bioRxiv preprint doi: https://doi.org/10.1101/057620; this version posted June 7, 2016. The copyright holder for this preprint (which was not certified by peer review) is the author/funder, who has granted bioRxiv a license to display the preprint in perpetuity. It is made available under aCC-BY-NC-ND 4.0 International license.

ISCs across the brain. The method is called functional segmentation ISC analysis (FuSeISC).[2] FuSeISC combines cluster analysis with ISC features extracted from multiple fMRI time series of multiple subjects, providing novel functional segmentation of the human brain. The fMRI time series can be either from separate experiments, separate runs within the same experiments, or extracted from selected time intervals of a longer fMRI experiment (for example, corresponding the scenes of a movie or an audio drama). FuSeISC takes both the extent and variability of the ISCs within the time series into account and performs the segmentation without *a priori* knowledge of the expected hemodynamic response due to stimulus. Moreover, FuSeISC does not constrain segmentation by any anatomic brain subdivision, allowing finding simultaneously both small clusters as well as anatomically dispersed larger functional network-like clusters. Finally, unlike many other segmentation/clustering methods, FuSeISC does not depend on selection of *ad hoc* user parameters, thereby making the method easy and straightforward to use.

The FuSeISC method described in this paper won the Study Forrest Real Life Cognition Challenge[3] [17] where the goal was to propose novel ways of analyzing complex fMRI data sets acquired under naturalistic stimulation. Here, we present the details of the algorithm and validate the technique more thoroughly with different data sets. FuseISC has been integrated to the ISC toolbox [18] and is freely available at `https://www.nitrc.org/projects/isc-toolbox/`.

## 2. Materials

### *2.1. ICBM Functional Reference Battery data*

The fMRI data collected during Functional Reference Battery (FRB) tasks developed by the International Consortium for Human Brain Mapping (ICBM) [19] was used for the evaluation of the method and for the construction of

[2] In addition to the term "functional segmentation", the term "functional parcellation" is often used for division of the brain into functionally distinct areas.

[3] `http://studyforrest.org/pages/challenge.html`,`http://studyforrest.org/contest_fuseisc.html`

bioRxiv preprint doi: https://doi.org/10.1101/057620; this version posted June 7, 2016. The copyright holder for this preprint (which was not certified by peer review) is the author/funder, who has granted bioRxiv a license to display the preprint in perpetuity. It is made available under aCC-BY-NC-ND 4.0 International license.

the simulated dataset described in the next subsection. The block-design FRB tasks are a set of behavioral tasks designed to reliably produce functional landmarks across subjects and as such they are ideal for the validation of functional segmentation methods. We have previously used the same data for other experiments and details of the data and experiments are provided in [9, 20], but, for convenience, we provide a short description here.

The FRB fMRI data were obtained from the ICBM database in the Image Data Archive of the Laboratory of Neuro Imaging. The ICBM project (Principal Investigator John Mazziotta, M.D., University of California, Los Angeles) is supported by the National Institute of Biomedical Imaging and BioEngineering. ICBM is the result of efforts of co-investigators from UCLA, Montreal Neurological Institute, University of Texas at San Antonio, and the Institute of Medicine, Jülich/Heinrich Heine University, Düsseldorf, Germany.

We extracted from the database the images of 41 right-handed subjects who had fMRI measurements for five FRB tasks: (1) auditory naming (AN) task, where the subject silently named objects that were verbally described; external ordering (EO) task, where the subject after a delay period (and thus relying on working memory) kept track of the abstract designs on the screen; (3) hand imitation (HA) task where the subject had to out his own hand into postures presented in pictures; (4) oculomotor (OM) task where the subject made saccades to target locations; and (5) verb generation (VG) task where the subject generated a verb that corresponded to an object presented on the screen. The detailed definitions of the five FRB tasks are available in the FRB software package[4] and in [9].

We discarded four subjects in a pre-screening phase because of poor data quality for at least one task in the battery. Thus, our final data set consisted of measurements from 37 healthy right-handed subjects (19 men and 18 women; mean age was 28.2 years and the age range 20–36 years). The functional fMRI data were collected with a 3 T Siemens Allegra FMRI scanner and the anatom-

[4] `http://www.loni.usc.edu/ICBM/Downloads/Downloads_FRB.shtml`

bioRxiv preprint doi: https://doi.org/10.1101/057620; this version posted June 7, 2016. The copyright holder for this preprint (which was not certified by peer review) is the author/funder, who has granted bioRxiv a license to display the preprint in perpetuity. It is made available under aCC-BY-NC-ND 4.0 International license.

ical T1 weighted MRI data with a 1.5 T Siemens Sonata scanner. The TR/TE times for the functional data were 4 s/32 ms, flip angle 90 °, pixel spacing 2 mm and slice thickness 2 mm. The acquisition parameters for the anatomical T1 data were 1.1 s/4.38 ms, 15 °, 1 mm and 1 mm, correspondingly. Preprocessing was performed by a standard FSL preprocessing pipeline including Gaussian 5 mm full width at half maximum (FWHM) spatial filtering. For more details, see [9].

### *2.2. Simulated data*

We generated synthetic fMRI data sets based on the ICBM data described above. Similarly to the experimental ICBM data, the simulated data consisted of five FRB tasks (AN, EO, HA, OM, and VG) from 37 subjects. The purpose of simulated data was to validate the functional segmentation method quantitatively when the true functional segmentation is fully known.

In the simulated data sets and for each task separately, every voxel was defined either as "activated" or "non-activated". Thus, any voxel was characterized by a 5-element binary vector creating $2^5 = 32$ distinct functional segments. Voxels were selected as "activated" according to the binarized statistical maps of the GLM analysis performed for the empirical ICBM data sets in [9] (thresholded at voxel-wise false discovery rate (FDR) corrected threshold $q = 0.001$). A simulated hemodynamic signal was included in the time series of the activated voxels. The signal was identical to the one used as a model in the GLM analysis of the data (see [9]), i.e., a boxcar convolved with a canonical hemodynamic response function (HRF). These signals were then corrupted by pink 1/f noise which was generated according to [21]. Signal-to-noise-ratio (SNR) was 0.02, which was quantified on the basis of the boxcar function *before* the convolution with the canonical HRF. All brain areas outside the activated regions contained only noise.

The simulation procedure was identical for every 37 simulated data sets and FRB tasks. We ignored anatomical and effect size variations between the subjects. Moreover, since the original empirical data sets were registered to the

bioRxiv preprint doi: https://doi.org/10.1101/057620; this version posted June 7, 2016. The copyright holder for this preprint (which was not certified by peer review) is the author/funder, who has granted bioRxiv a license to display the preprint in perpetuity. It is made available under aCC-BY-NC-ND 4.0 International license.

MNI-152 coordinate space, we did not perform registration or motion correction as preprocessing. The preprocessing only included Gaussian 5 mm FWHM spatial filtering.

### *2.3. StudyForrest data*

To demonstrate FuSeISC method with naturalistic stimulation, we analyzed fMRI data sets of 19 subjects provided by the organization committee of the StudyForrest project and data challenge. The details of the experiment, data collection and preprocessing are provided by [17]. In brief, the participants listened to a German sound track (Koop, Michalski, Beckmann, Meinhardt & Benecke, produced by Bayrischer Rundfunk, 2009) of the movie "Forrest Gump" (R. Zemeckis, Paramount Pictures, 1994) as broadcast as an additional audio track for visually impaired listeners on Swiss public television.

The audio content was largely identical to the dubbed German sound track of the movie, including the original dialogues and environmental sounds, but then added by interspersed narrations by a male speaker who described the visual contents of the scenes. As detailed by [17], the participants listened to the movie sounds using custom-built in-ear headphones designed to maximize comfort during the scanning. T2-weighted echo-planar images (gradient-echo, 2s TR, 22 ms echo time 0.78 ms echo spacing, generalized autocalibrating partially parallel acquisition (GRAPPA)) were acquired during stimulation using a whole-body 7T Siemens MAGNETOM scanner. 36 axial slices (thickness 1.4 mm 1.4 x 1.4 mm in-plane resolution 224 mm field-of-view, anterior-to-posterior phase encoding direction) with 10% interslice gap were recorded in ascending order. Slices were oriented to include the ventral portions of frontal and occipital cortex while minimizing the intersection with the eyballs.

The entire data set consisted of 8 runs (about 15 min each) for each subject from which we selected five highly attractive audio segments for our analysis. We ranked the attractiveness of the clips based on an simple internet survey of the corresponding video clips (that the subjects did not see) on online video services such as YouTube and movie discussion forums. The time points used

bioRxiv preprint doi: https://doi.org/10.1101/057620; this version posted June 7, 2016. The copyright holder for this preprint (which was not certified by peer review) is the author/funder, who has granted bioRxiv a license to display the preprint in perpetuity. It is made available under aCC-BY-NC-ND 4.0 International license.

to create the five clips are listed in supplementary material (Section 1, Table S1). The exact data set for the analysis was extracted from the original preprocessed linear anatomical alignment set of the StudyForrest data. In addition to preprocessing performed by [17], we included Gaussian spatial filtering with isotropic 3 mm FWHM.

## 3. Methods

The FuSeISC method consists of two main steps:

1. **Feature extraction** (Section 3.1): Given $M$ fMRI time series of $N$ subjects, $2M$ ISC-based features are extracted for each voxel as illustrated in Fig. 1.
2. **Clustering** (Section 3.2): Feature vectors of the voxels are clustered to form the functional segmentation of the brain.

These steps together with the performance evaluation metrics used will be described next.

### *3.1. Feature extraction*

Functional segmentation has been typically performed individually for each subject based on the individual fMRI time series, and the individual clustering results have been combined in a subsequent stage to form group-level cluster maps (see, e.g., [22]). We propose a different approach in which we directly integrate information across subjects by computing subject-pairwise ISCs from multiple temporally distinct time series and extracting features from them. Two types of ISC statistic/features are extracted from selected time-series: 1) mean and 2) variability of subject-pairwise correlations. The use of both mean and variability features is useful because they provide complementary information about processing in different brain regions during selected time-series (e.g. video/audio clips) of interest. For instance, *high mean ISC* alone suggests that processing is coherent among subjects (subject-pairwise correlations have systematically high values) whereas *low mean and low variability* in ISCs (subject

bioRxiv preprint doi: https://doi.org/10.1101/057620; this version posted June 7, 2016. The copyright holder for this preprint (which was not certified by peer review) is the author/funder, who has granted bioRxiv a license to display the preprint in perpetuity. It is made available under aCC-BY-NC-ND 4.0 International license.

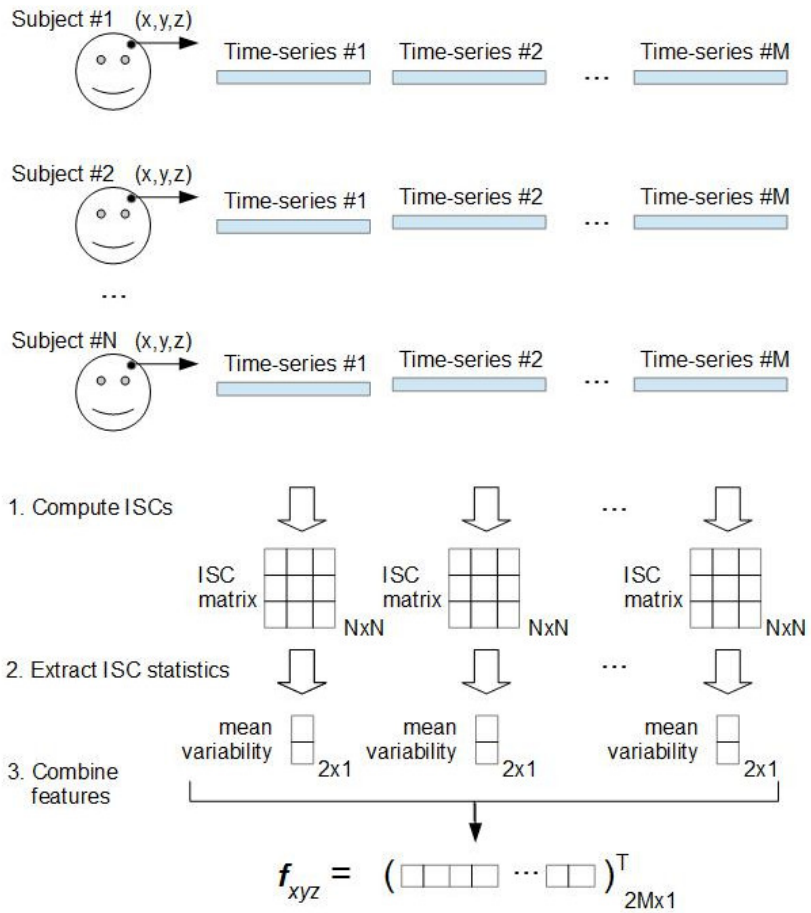


Figure 1: Illustration of the feature extraction in FuSeISC for one arbitrary voxel located at a coordinate (x,y,z). At first, $M$ ISC matrices are independently computed based on the fMRI time series of $N$ subjects. In our study, the total number of time series was $M = 5$, corresponding to the total number of tasks (ICBM data) or movie clips (StudyForrest data) of interest. From each $N \times N$ ISC matrix, two features, mean and variability, are extracted using the Jackknife procedure. These features are stacked into a single feature vector $f_{xyz}$, whose dimension is $2M$. This procedure is repeated for each brain voxel to obtain altogether 228,483 and 449,612 feature vectors for cluster analysis, corresponding to the ICBM and StudyForrest data, respectively.

bioRxiv preprint doi: https://doi.org/10.1101/057620; this version posted June 7, 2016. The copyright holder for this preprint (which was not certified by peer review) is the author/funder, who has granted bioRxiv a license to display the preprint in perpetuity. It is made available under aCC-BY-NC-ND 4.0 International license.

pairwise correlation values are likely close to zero) is less interesting and may simply indicate noise. On the other hand, *low mean and high variability* in ISCs (both high and low subject-pairwise correlations are present) suggests active processing together with high inter-individual differences. This information cannot be discovered using traditional ISC methods relying on mean information.

In more detail, feature extraction was performed separately for each voxel across the brain using the ISC toolbox [18] as described in Figure 1. For each of $M$ time series, we computed correlation coefficients between the time series of all subject pairs, leading to $N \times N$ ISC matrix for each time series, where $N$ is the number of subjects. For instance, the fMRI data sets of the Forrest study were divided in $M = 5$ distinct time series, corresponding to the five scenes of interest (see Section 2.3 on how the most interesting scenes were selected). The ISC features were computed based on the ISC matrices. First, the means of subject-pair-wise correlation coefficients, i.e., *mean ISC features*, were computed:

$$\bar{r}(m) = \frac{1}{N(N-1)/2} \sum_{i=1}^{N} \sum_{j=2, j>i}^{N-1} r_{ij}(m), \tag{1}$$

where $\overline{r}(m)$ denotes a group-level ISC in a given voxel (a voxel index is omitted for clarity) for time series $m$ and $r_{ij}(m)$ is the correlation coefficient between $m$th fMRI time-courses of subjects $i$ and $j$. Note that because $r_{ii}(m) = 1$ and $r_{ij}(m) = r_{ji}(m)$, it is sufficient to compute correlation coefficients across $N(N-1)/2$ subject pairs (instead of $N^2$ pairs). Such pairwise averaged ISC is a common way to represent ISC maps [18]. We computed *variability ISC features* using a leave-one-subject-out Jackknife procedure similar to that applied by [20]. More specifically, we first computed mean ISC values so that each subject was left out from the original sample one at a time. This procedure corresponds to the computation of the $N$ mean ISC values, termed *pseudovalues*, for $i$=1,2,...,$N$, so that $i$th row and $i$th column in the ISC matrix are left out one at a time. The Jackknife standard error estimate was then computed

bioRxiv preprint doi: https://doi.org/10.1101/057620; this version posted June 7, 2016. The copyright holder for this preprint (which was not certified by peer review) is the author/funder, who has granted bioRxiv a license to display the preprint in perpetuity. It is made available under aCC-BY-NC-ND 4.0 International license.

as standard deviation of the pseudovalues multiplied by $\sqrt{N-1}$. With simple algebraic manipulation, it can be shown that this procedure corresponds to computing

$$\hat{r}_J(m) = \frac{2}{(N-2)}\sqrt{\frac{N-1}{N}\sum_{i=1}^{N}(\bar{r}_i(m) - \bar{r}(m))^2}, \tag{2}$$

where $\bar{r}_i(m) = \frac{1}{N-1}\sum_{j\neq i} r_{ij}(m)$. Finally, the mean and variability features were combined into the feature vector

$$\mathbf{f} = [\bar{r}(1), \hat{r}_J(1), \ldots, \bar{r}(M), \hat{r}_J(M)]^T.$$

Our approach does not only reduce the dimension of the original data set drastically but allows for novel interpretation of group fMRI data sets. The supporting idea is that the voxels showing similar mean and variability statistics in ISCs for each time-series of interest belong to the same functional segment. This way, the brain can be divided in different regions such as in those having high mean and high variability in ISCs, and those having low mean and high variability in ISCs. Because time-series of interest have different characteristics in ISCs, it is likely that clustering based on all the continuous-valued ISC features reveals multiple brain areas with specific ISC characteristics. It is insightful to analyze these found segments together with their specific ISC characteristics.

### *3.2. Robust functional segmentation algorithm*

*Gaussian mixture model*

After the feature extraction, we learned a Gaussian mixture model (GMM) to cluster the ISC features. GMM provides a principled way of performing the functional segmentation under the assumption that the ISC features form clusters which follow a Gaussian distribution. Importantly, we did not impose any spatial constraints on our model, meaning that functional segments need not be spatially contiguous but can consist of several spatially disjoint "subclusters". The model is given by [23]:

bioRxiv preprint doi: https://doi.org/10.1101/057620; this version posted June 7, 2016. The copyright holder for this preprint (which was not certified by peer review) is the author/funder, who has granted bioRxiv a license to display the preprint in perpetuity. It is made available under aCC-BY-NC-ND 4.0 International license.

$$p\left(\mathbf{f}|\boldsymbol{\theta}\right) = \sum_{i=1}^{C} w^{(i)} g\left(\mathbf{f}|\boldsymbol{\mu}^{(i)}, \boldsymbol{\Sigma}^{(i)}\right), \tag{3}$$

where $C$ is the total number of clusters, $\mathbf{f} \in \mathbb{R}^{2M}$ feature vector described in the previous section, $\boldsymbol{\theta}$ denotes all the parameters of the model, $w^{(i)} \in [0, 1]$, $\sum_i w^{(i)} = 1$ are mixture weight parameters, and $g\left(\mathbf{f}|\boldsymbol{\mu}^{(i)}, \boldsymbol{\Sigma}^{(i)}\right)$ are multivariate Gaussian component densities with the mean $\boldsymbol{\mu}^{(i)}$ and the covariance $\boldsymbol{\Sigma}^{(i)}$. Because a multivariate Gaussian distribution can be fully described by its mean and covariance matrix, the unknown parameters of the GMM are $\boldsymbol{\theta} = \left\{w^{(i)}, \boldsymbol{\mu}^{(i)}, \boldsymbol{\Sigma}^{(i)}\right\}$, for $i = 1, 2, \ldots, C$. The elements of $\boldsymbol{\mu}^{(i)} \in \mathbb{R}^{2M}$ are given by $\mu_j^{(i)}$ and the elements of $\boldsymbol{\Sigma}^{(i)} \in \mathbb{R}^{2M \times 2M}$ are given by $\sigma_j^{(i)}$. We estimated the maximum likelihood solutions for these parameters using the expectation maximization (EM) algorithm [24, 23] implemented in the Statistics Toolbox of the Matlab.

*Finding initial model*

A major difficulty with the GMM-based clustering is that the quality of the clustering is highly dependent on a selected initial model [25, 26]: if the mean vectors of the Gaussian components are not initially near true cluster mean values, the EM algorithm converges towards a suboptimal solution and easily misses interesting clusters in the data[5]. Another problem is that the total number of clusters $C$ in the GMM is hard to determine because well-known model selection criteria, such as the Bayesian information criterion (BIC), tend to overestimate the total number of clusters in complex fMRI data sets [27].

To overcome these problems, we propose restricting a set of initial candidate models *a priori* to meaningful ones based on local structures in the data. Besides accuracy, prerequisites for the algorithm are computational and memory efficiency, because we run segmentation across all the brain voxels (the number

[5]This difficulty follows from the non-convexity of the maximum likelihood cost function to be minimized and every local optimization algorithm (including gradient methods) have this problem.

bioRxiv preprint doi: https://doi.org/10.1101/057620; this version posted June 7, 2016. The copyright holder for this preprint (which was not certified by peer review) is the author/funder, who has granted bioRxiv a license to display the preprint in perpetuity. It is made available under aCC-BY-NC-ND 4.0 International license.

of brain voxels was 228,483 for the ICBM data and 449,612 for the StudyForrest data). Here is a summary of the algorithm:

- Compute a $k$-nearest neighbor ($k$-NN) list for each data point.
- Compute a weighted *shared nearest neighbor* (SNN) graph [28] of the data based on the $k$-NN list. In the SNN graph, two data points are connected only if they belong to each others' nearest neighbor lists.
- From this graph, extract a high number of subgraphs by sparsification.
- Compute mean vectors of the connected components in each subgraph. This leads to multiple sets of GMM mean vector candidates.
- Choose a best set of initial mean vectors and estimate corresponding covariance matrices according to a minimum distance rule.

See Appendix A.1 for more details. The method was validated against state-of-the-art-algorithms, such as Ward's method [29], $K$-means [30], $K$-means++ [31] and Affinity propagation [32]. The validation results are presented in supplementary material (Section 3).

The proposed method is dependent on a single user parameter: a neighborhood size $k$. This parameter describes how many neighboring feature vectors (voxels) are used to form the SNN graphs.[6] A choice of $k$ affects the total number of clusters indirectly: Smaller values of $k$ lead to large number of small clusters and thus can describe fine details in the original data. However, too detailed segmentation is difficult to analyze visually. Larger values of $k$ lead to a lower number of clusters but more details in the data are lost. Thus, a choice of $k$ is a compromise between fine-graininess and interpretability of the findings. In this sense, $k$ is not an ad hoc parameter but rather determines granularity level of the analysis.

We selected $k$ based on the following analysis: at first, we run FuSeISC for several values of $k$. Then, we plotted the total number clusters as a function

[6] It is important to note that the connected components of the SNN graph are found in a *feature space* and not in a spatial domain and this way a single cluster may consist of multiple spatially connected components (subclusters).

bioRxiv preprint doi: https://doi.org/10.1101/057620; this version posted June 7, 2016. The copyright holder for this preprint (which was not certified by peer review) is the author/funder, who has granted bioRxiv a license to display the preprint in perpetuity. It is made available under aCC-BY-NC-ND 4.0 International license.

of $k$ and select a value from the region where the number of clusters remains relatively constant (see Section 4 in supplementary material for validity of this approach using synthetic data). To confirm that the selected $k$ value was appropriate, we also computed the similarity (using the adjusted rand index ARI; see Section 1 in supplementary material) between all FuSeISC solutions constructed from different values of $k$. In the constructed "stability matrix", we looked for stable region of high ARI values, because in this region the segmentation results were similar irrespective of the choice of $k$. As a final solution, we picked $k$ from the region which shows stability in terms of both the total number of clusters and ARI.

### *3.3. Code availability*

FuseISC has been integrated to the ISC toolbox [18] and is freely available at `https://www.nitrc.org/projects/isc-toolbox/`.

## 4. Results

### *4.1. Spatial organization of the clusters*

It is insightful to compare FuSeISC results with "conventional" univariate ISC results. For this purpose, we computed conventional ISC maps across each five clip of interest for the StudyForrest data using the ISC toolbox [18]. Thresholds for statistical significance were determined using a resampling procedure implemented in the toolbox. The thresholds were multiple comparison corrected across the voxels using the FDR ($q < 0.001$). Figure 2(A) shows three axial slices of the ISC map computed across the Clip0. Here, a colormap denotes an average ISC computed across all subject-pairwise ISCs. The highest ISC is visible in the auditory cortex, which is natural because the stimuli was provided auditorily. Interestingly, however, also frontal cortex shows statistically significant ISC. Figure 2(B) provides an overview of the ISCs elicited by all the five clips. In this representation, red color denotes statistically significant ISC during Clip0, green color shows statistically significant ISC during Clip1, and

bioRxiv preprint doi: https://doi.org/10.1101/057620; this version posted June 7, 2016. The copyright holder for this preprint (which was not certified by peer review) is the author/funder, who has granted bioRxiv a license to display the preprint in perpetuity. It is made available under aCC-BY-NC-ND 4.0 International license.

so on. (When several clips elicited significant ISC in the same voxel, the color code corresponding to the clip with the highest ISC is shown.) All the clips revealed statistically significant ISC in the auditory cortex, but spatial location of ISCs also partly varied depending on the clip. For instance, Clip0 showed ISC in frontal regions whereas Clip2 showed ISCs in the visual cortex.

Figure 2(C) shows a FuSeISC map of the same data using a neighborhood size parameter $k$=230 after discarding irrelevant clusters (see Section 4.3 how we selected neighborhood sizes for the StudyForrest and ICBM data and discarded irrelevant clusters). As conventional ISC mapping simply provides information which voxels show statistically significant average ISC across subject pairs for different clips, FuSeISC segments the brain into functionally distinct clusters. These clusters are formed on the basis of both average and variability features of the subject-pairwise ISCs extracted from each clip. Each cluster is shown in different color, and the names of the brain regions corresponding to the center of mass of the clusters are listed next to the colorbar. Clusters are organized in the decreasing order of the overall ISC of the clips. The names of the largest and the second largest subclusters are provided.[7] For a more comprehensive listing of brain regions for each cluster, see supplementary material (Section 1, Table S4).

FuSeISC provided physiologically feasible functional division, with clusters in auditory and visual cortices. Many of the clusters were spatially contiguous and/or symmetric between the hemispheres, suggesting that clusters characterize neuroscientifically plausible information instead of noise. Interestingly, FuSeISC revealed brain areas that remained undetected by the conventional ISC. For instance, a frontal region covered by cluster #13 was not covered by ISC maps of the individual clips in Fig. 2(B). Thus FuSeISC seemed to be more

[7] Because spatial constraints are not used in FuSeISC, each found cluster in a feature space can consist of more than one spatially disjoint subclusters. The name of the second largest subcluster is reported only when the actual cluster consists of at least two spatially disjoint subclusters whose sizes are greater than 100 voxels. Moreover, if the center of mass is located in white matter or non-specified brain area, the largest cortical brain region intersecting with the cluster is reported instead of the location of the center of mass.

bioRxiv preprint doi: https://doi.org/10.1101/057620; this version posted June 7, 2016. The copyright holder for this preprint (which was not certified by peer review) is the author/funder, who has granted bioRxiv a license to display the preprint in perpetuity. It is made available under aCC-BY-NC-ND 4.0 International license.

sensitive than the conventional ISC mapping for detecting activated brain areas. Moreover, FuSeISC finds these areas in a fully data-driven manner without the requirement for selecting a threshold value for statistical significance.

Figure 3 provides a more comprehensive view of the FuSeISC results. Figure 3(A) shows the clusters of the ICBM data. Visual cortices were segmented to multiple areas, similarly as by applying independent component analysis (ICA) to fMRI data obtained during natural viewing [33], with different segments for foveal and peripheral vision, for example. Separate clusters also covered the intraparietal sulcus bilaterally, V5, extrastriatal body area, and parahippocampal space area. Interestingly, the segmentation also seemed to delineate parts of the resting-state network (with the nodes of the "default-mode network" in posterior parietal cortex and medial prefrontal cortex).

Figure 3 (B) shows the clusters of the StudyForrest data. Interestingly, the clustering along the perisylvian region showed subsegmentation of the segmentation using ICBM data. For example, the supratemporal auditory cortex was separated from the larger perisylvian cluster, as well as from a cluster in the temporoparietal junction. Even in these data, the reactivity of mesial "default-mode network" showed up (see also [34]).

In general, the found patterns in both the ICBM and StudyForrest data covered large parts of both the convexial and mesial cortex. The clusters seemed physiologically feasible, crudely resembling, e.g., the patterns previously seen with ICA of various tasks. Many clusters were bilaterally symmetric. As the StudyForrest data was of higher resolution and smoothing kernel had smaller FWHM than with ICBM data, some of the clusters were more fragmented spatially than the clusters of the ICBM data, but the clusters still formed clear spatial patterns in the cortex. The complete 3D spatial maps of clustering results are available in the NeuroVault service [35] at `http://www.neurovault.org/collections//PXNGFJTL/`.

bioRxiv preprint doi: https://doi.org/10.1101/057620; this version posted June 7, 2016. The copyright holder for this preprint (which was not certified by peer review) is the author/funder, who has granted bioRxiv a license to display the preprint in perpetuity. It is made available under aCC-BY-NC-ND 4.0 International license.

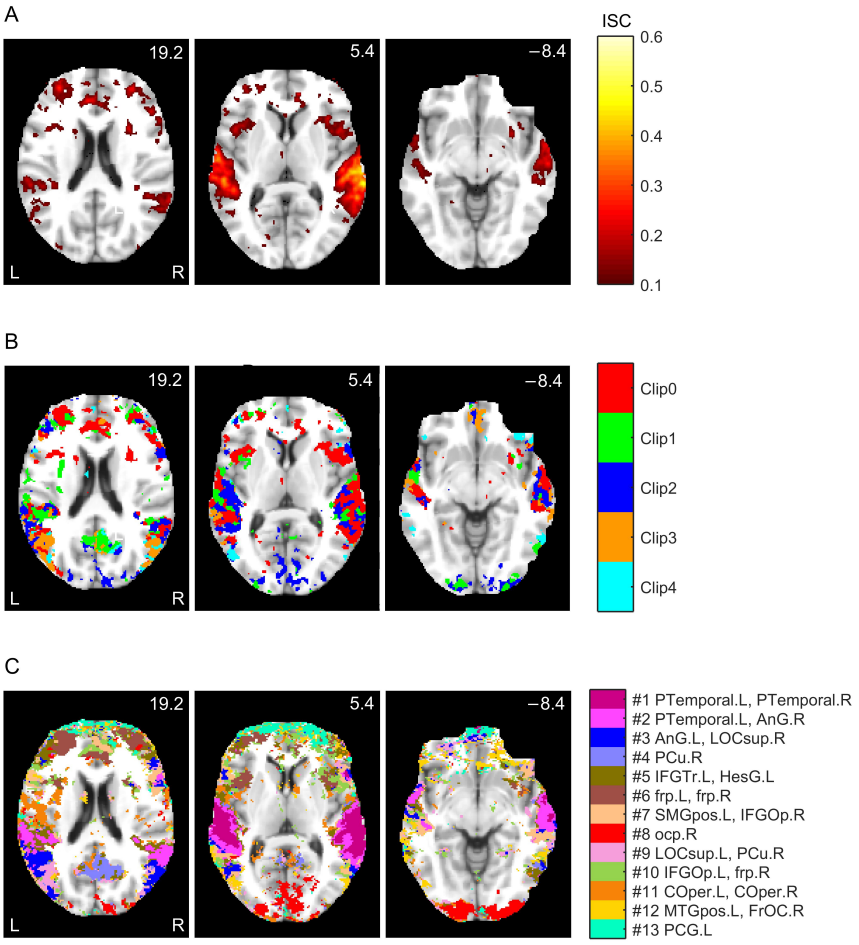


Figure 2: Comparison between conventional ISC and FuSeISC results for the StudyForrest data: (A) ISC map of the Clip0, (B) Integrated ISC map of the five clips, and (C) FuSeISC map of the five clips. The axial slices are presented in millimeters in the MNI coordinates. The ISC maps were FDR corrected at $q < 0.001$ across all the voxels. FuSeISC does not require threshold selection, but clusters located dominantly over cerebral white matter, brain-stem, or ventricular areas were discarded. Note how FuSeISC found spatially meaningful segmentation and revealed more brain areas than conventional univariate ISC mapping.

bioRxiv preprint doi: https://doi.org/10.1101/057620; this version posted June 7, 2016. The copyright holder for this preprint (which was not certified by peer review) is the author/funder, who has granted bioRxiv a license to display the preprint in perpetuity. It is made available under aCC-BY-NC-ND 4.0 International license.

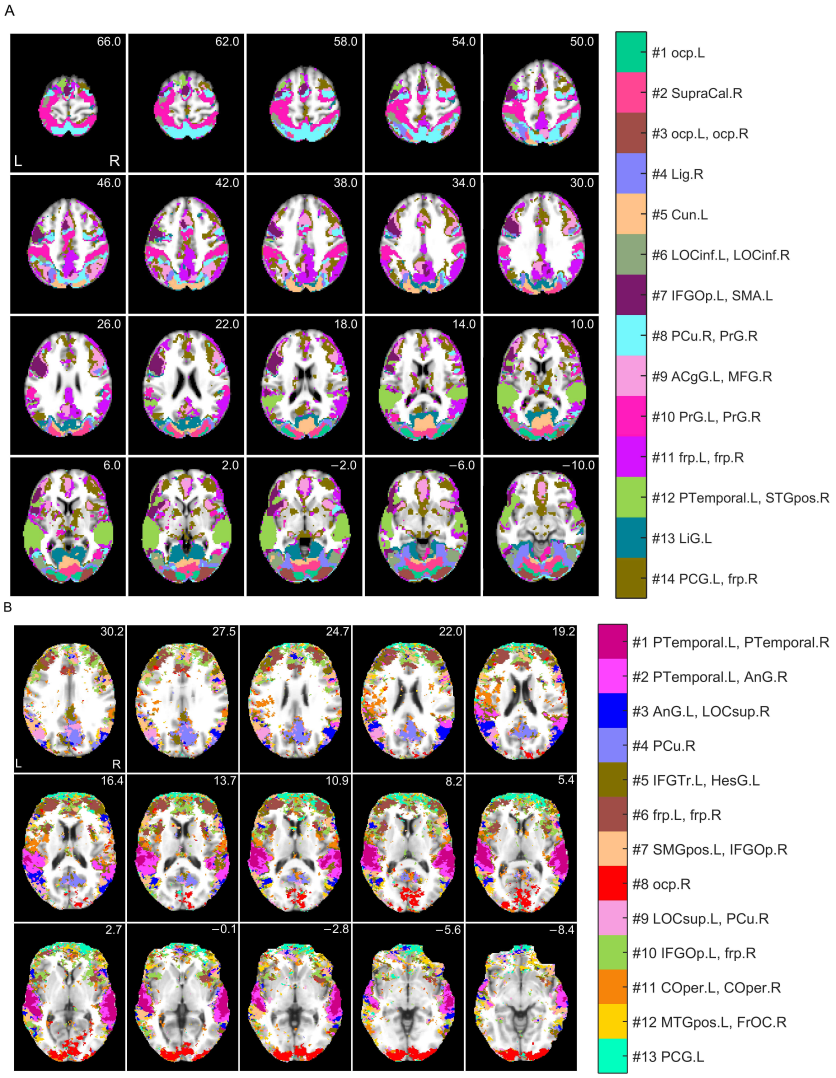


Figure 3: Functional segmentation of the (A) ICBM and (B) StudyForrest data by FuSeISC. The axial slices are presented and labeled with millimeters in the MNI coordinates. For the abbreviations of the brain region names and the spatial coordinates of the cluster centers, see supplementary material (Section 1, Tables S2-S4).

bioRxiv preprint doi: https://doi.org/10.1101/057620; this version posted June 7, 2016. The copyright holder for this preprint (which was not certified by peer review) is the author/funder, who has granted bioRxiv a license to display the preprint in perpetuity. It is made available under aCC-BY-NC-ND 4.0 International license.

### *4.2. ISC information of the clusters*

Figure 4 shows cluster-specific ISC information (mean and across subject pair variability) obtained by the FuSeISC. Figure 4(A) shows the values of mean ISCs feature (cluster average vectors) $\mu_j^{(i)}$, $j = 1, 3, 5, 7, 9$, for each cluster $i$ as colored bar plots for the ICBM data. Specific colors in the bar graphs correspond to different tasks (AN, EO, HA, OM, VG) and the heights of the bars correspond to the values of the mean ISC features. Error bars denote the standard deviations $\sigma_{jj}^{(i)}$ of the clusters obtained from the learned covariance matrices (these should not be confused with the variance ISC features). The clusters with the highest mean ISC were located around the occipital cortex. Note how the AN (red color) task elicited less ISC than the other tasks in nearly all clusters. The major exception is the cluster located in auditory regions (#12 PTemporal.L, STGpos.R), where ISCs of the AN task were dominant in contrast to the other tasks. This is physiologically plausible because AN was the only task in which the stimuli were presented auditorily. In a similar fashion, the HA (blue color) task exhibited dominant ISCs in the cluster #10 (PoG.L, PrG.R). This is physiologically plausible, because the cluster is located around the sensorimotor strip. Figure 4(B) shows the corresponding plot for the StudyForrest data for the five clips of interest. The clusters with the highest mean ISC were located in the auditory cortex.

Figures 4(C) and 4(D) show the corresponding bar graphs for the ISC variability features: $\mu_j^{(i)}$, $j = 2, 4, 6, 8, 10$. Clearly, for the ICBM data, variability in ISC (see Fig. 4(C)) decreased together with the mean ISC (see Fig. 4(A)). In fact, the correlation coefficient between the mean and variability feature across clusters was very high (0.94), indicating that the variability features did not add important information to mean ISC features for simple block design data. For the StudyForrest data, situation is different: variability in ISCs was considerably higher and the correlation between ISC variability and mean feature values was much lower (0.75) than in the case of ICBM data. These findings are interesting, suggesting that variability in ISCs contain meaningful information in fMRI data sets collected in naturalistic experiments.

bioRxiv preprint doi: https://doi.org/10.1101/057620; this version posted June 7, 2016. The copyright holder for this preprint (which was not certified by peer review) is the author/funder, who has granted bioRxiv a license to display the preprint in perpetuity. It is made available under aCC-BY-NC-ND 4.0 International license.

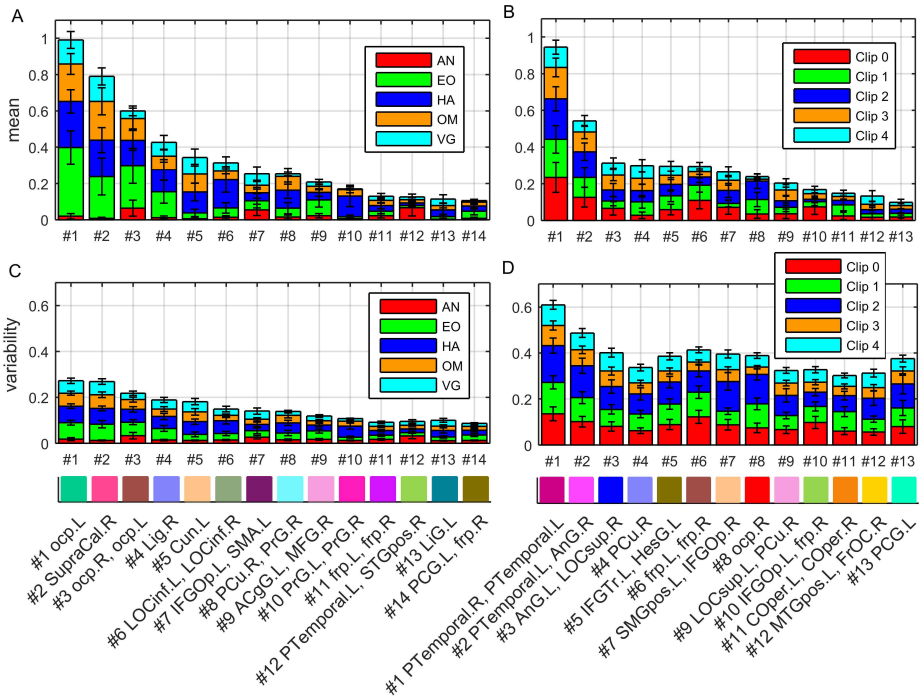


Figure 4: Cluster-specific information extracted from the estimated distribution parameters of the GMM: (A) ISC mean of the ICBM data, (B) ISC mean of the StudyForrest data, (C) ISC variability of the ICBM data, and (D) ISC variability of the StudyForrest data. See Table S2 in supplementary material for the abbreviations of the brain region names. The values of the model parameters are stacked on top of each other with different colors corresponding to tasks/clips of interest. Clusters are organized in the decreasing order of the mean ISC and their names and colors corresponds to Fig. 3. Both data sets contain clusters with widely different mean ISCs. For the ICBM data, ISC variability is low and highly correlated with the mean ISC data across clusters. For the StudyForrest data, ISC variability is much higher and provides complementary information for ISC mean. This underlines the usefulness of FuSeISC in the analysis of fMRI data collected in naturalistic experiments.

bioRxiv preprint doi: https://doi.org/10.1101/057620; this version posted June 7, 2016. The copyright holder for this preprint (which was not certified by peer review) is the author/funder, who has granted bioRxiv a license to display the preprint in perpetuity. It is made available under aCC-BY-NC-ND 4.0 International license.

### *4.3. Selection of final segmentations*

We describe how we selected $k$ to obtain the final FuSeISC maps shown in the previous section. First, we ran FuSeISC for several values of $k$ and plotted the total number clusters for each result. Then, we found the range of stable values of $k$ leading to a constant number of clusters. Figure 5(A) shows the total number of clusters found for real ICBM and StudyForrest data sets as a function of a neighborhood size $k$. Interestingly, the curves were highly similar to each other. With small $k$-values the number of clusters was high but the number decreases rapidly as $k$ became larger. When $k \geq 230$, the number of clusters in the ICBM data stabilized around 20. For the StudyForrest data, the number of clusters in a stable region was approximately the same.

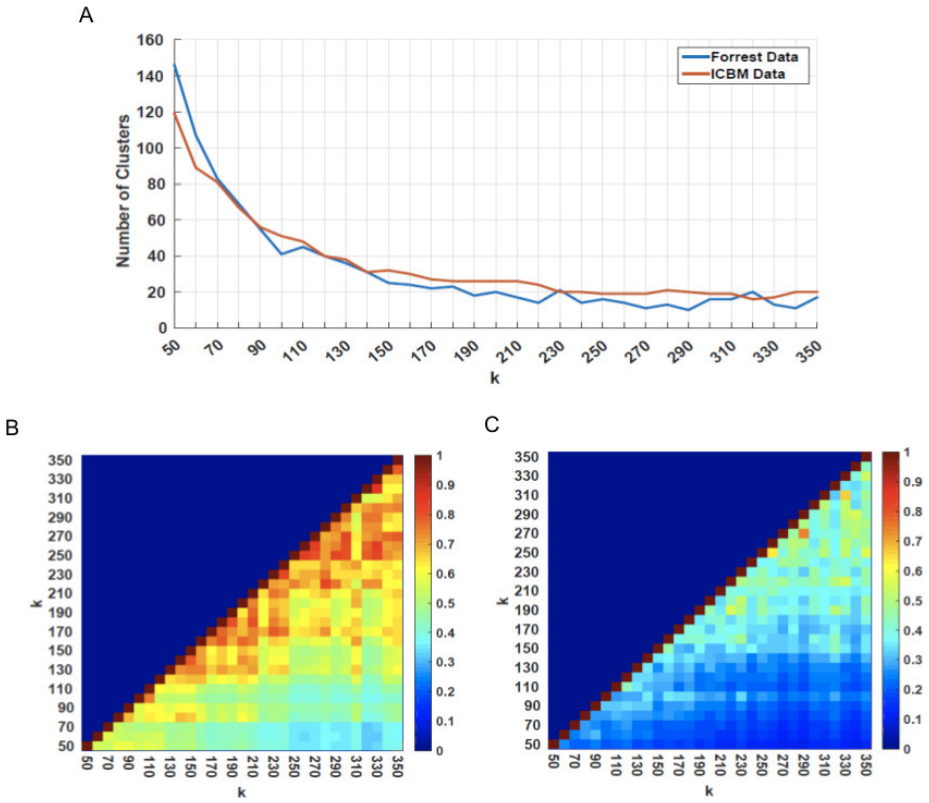


Figure 5: The effect of neighborhood size for the clustering results of the fMRI data: A) Total number of clusters of the ICBM and StudyForrest data, B) ARI stability matrix of the ICBM data, and C) ARI stability matrix of the StudyForrest data.

bioRxiv preprint doi: https://doi.org/10.1101/057620; this version posted June 7, 2016. The copyright holder for this preprint (which was not certified by peer review) is the author/funder, who has granted bioRxiv a license to display the preprint in perpetuity. It is made available under aCC-BY-NC-ND 4.0 International license.

In addition, we computed ARI between results obtained for different values of $k$. In the resulting stability matrix, a high ARI value indicates that the segmentation result is stable, i.e., similar for two different choices of $k$. Figures 5(B) and (C) show the ARI stability matrices for the ICBM data and StudyForrest data, respectively. For both data sets, highest similarities were found between solutions where $k$ was relatively large. The ARI values of the StudyForrest data were slightly lower than those of the ICBM data, but this is natural because the spatial resolution (and the total number of voxels) in the StudyForrest data was notably higher.

Based on the above findings, we selected one of the stable solutions from both data sets for closer inspection ($k$=250 for the ICBM data and $k$=230 for the StudyForrest data). In these solutions, the exact number of clusters were 19 for the ICBM data and 21 for the StydyForrest data. Out of these clusters, we discarded clusters dominantly located over cerebral white matter, brainstem, or ventricular areas (the rejection thresholds were 5,000 voxels and 10,000 voxels for the ICBM and StudyForrest data, respectively). The purpose of this procedure was to make the visual investigation of more interesting clustering easier. After this post-processing, the total number of clusters were 14 for the ICBM data and 13 for the StudyForrest data.

### *4.4. Simulation data*

To validate our approach, we analyzed the simulated ICBM data and compared its results with the ground truth as well as with the real data sets. Figure 6(A) presents the performance of the functional segmentation for the simulated ICBM data against the ground truth as a function of the neighborhood size $k$. For a wide range of parameters, ARI values resulted in "moderate agreement" (ARI between 0.4–0.6) between the ground truth and the estimated cluster labeling computed across the 72,577 voxels that were activated in the ground truth for at least one task. However, FuSeISC was run across the entire brain involving 449,612 voxels to make the clustering task realistic.

Figure 6(B) shows the total number of clusters as a function of $k$. Clearly, the

bioRxiv preprint doi: https://doi.org/10.1101/057620; this version posted June 7, 2016. The copyright holder for this preprint (which was not certified by peer review) is the author/funder, who has granted bioRxiv a license to display the preprint in perpetuity. It is made available under aCC-BY-NC-ND 4.0 International license.

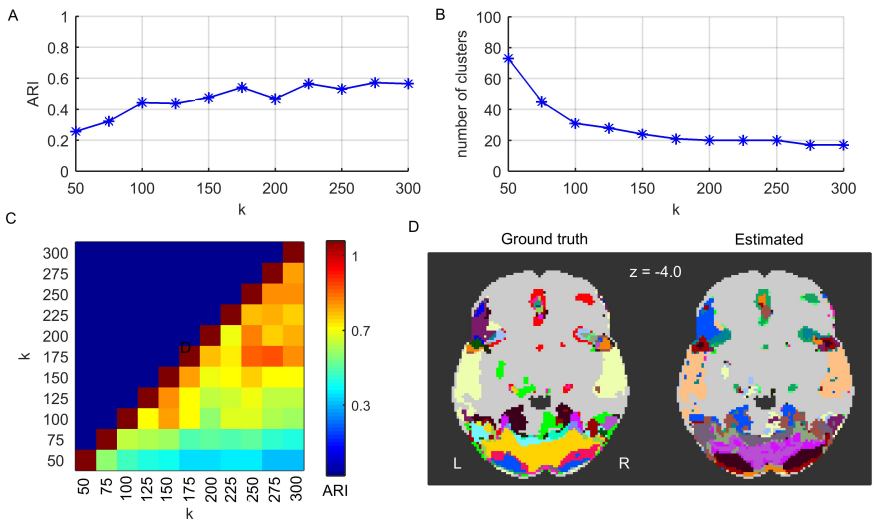


Figure 6: Results of the FuSeISC for the simulated ICBM data: A) clustering quality, B) total number of clusters, C) stability of the results, and D) an example slice showing spatial organization of the clusters (both ground truth and estimated clusters are shown).

curve shows a region of constant number of clusters (20) when $200 \leq k \leq 250$. This corresponded well with the real data results (see Fig. 5B), where the stable regions also consisted of about 20 clusters.

Figure 6(C) shows an ARI stability matrix of the solutions. This matrix shows the similarity between segmentation results computed for different values of $k$. Clearly, segmentation results were stable within the aforementioned constant region, since the ARI values were high (red color in the stability matrix indicates high similarity between results).

Figure 6(D) shows a spatial organization of the clusters for one stable result ($k = 225$) and one axial slice ($z = -4.0$ mm in MNI). The ground truth segmentation (left) and the estimated segmentation (right) are shown side by side to allow comparison between the maps. Based on visual inspection, the estimated segmentation resembles the true segmentation in most regions very well[8].

[8]Note that the spatial organization of the colors across the two maps is arbitrary — only differences and similarities in the actual segmentation should be compared.

bioRxiv preprint doi: https://doi.org/10.1101/057620; this version posted June 7, 2016. The copyright holder for this preprint (which was not certified by peer review) is the author/funder, who has granted bioRxiv a license to display the preprint in perpetuity. It is made available under aCC-BY-NC-ND 4.0 International license.

## 5. Discussion

### *5.1. Functional feasibility of the segmentation*

The examination of the analysis results for the real fMRI data results in a couple of observations. First, the clusters for the 5-task ICBM dataset covered most of the convexial and mesial cortex, thereby clearly extending the typical ISC maps that tend to concentrate on early sensory processing areas because the correlations between the subjects' fMRI time series are strongest there [12]. The decrease of ISC in the higher levels of the processing hierarchy is evident also in group-ICA results of fMRI obtained during natural viewing: the reconstruction of individual time courses shows considerably more inter-individual variability at, e.g., parieto-occipital sulcus than at early visual cortices [36].

Second, the segmentation gives an impression of a division that could be physiologically feasible, with clusters in auditory and visual cortices. Many of the clusters are symmetric between the hemispheres. The segmentation also seems to delineate parts of the resting-state network. Although this network is considered to be highly "intrinsic" [2], it likely reacts synchronously in different subjects to the task demands.

The same 5-task ICBM dataset as used in this work has been analyzed previously task-by-task for comparing the GLM and the conventional ISC [9] for the purpose of the ISC method validation. The analysis demonstrated that the activation areas detected by the ISC (with no knowledge of the reference time course for the stimuli) and GLM (with a reference time course) were highly overlapping. In this work, all the tasks were analyzed jointly and one may thus ask whether the results would differ from just a combination of task-wise analysis. In this sense, the visually most apparent difference was that the FuSeISC allowed the segmentation of visual cortex into multiple areas, as described above, whereas in the conventional analysis all the tasks with the visual input (VG, OM, HA, EO) activated a large part of the visual cortex and there was a little difference in the activation regions between the tasks.

bioRxiv preprint doi: https://doi.org/10.1101/057620; this version posted June 7, 2016. The copyright holder for this preprint (which was not certified by peer review) is the author/funder, who has granted bioRxiv a license to display the preprint in perpetuity. It is made available under aCC-BY-NC-ND 4.0 International license.

### *5.2. Variability ISC features*

A common practice in neuroimaging studies is to improve SNR by averaging results across subjects [37]. Such an approach is based on a restrictive assumption that subjects process information similarly. Although this approach has increased our understanding in brain processes which are similar across subjects, it cannot help us to understand individual brain processing because this type of group-averaging does not only remove noise but also information regarding inter-subject variability [14, 38]. FuSeISC allows detection of brain regions on the basis of both group-average (mean ISC features) and inter-subject variability (variability ISC features) information and, in this way, inherently assumes inter-individual variation between subjects.

High mean ISC features are interesting because they indicate that processing is similar across subjects on average. But also brain regions eliciting high variability in subject-pairwise ISCs is interesting, because this indicates similarity in processing between some subject pairs and dissimilarity between others (this is because high variability is only achieved when both high and low pairwise ISCs are present). FuSeISC can reveal these regions and may this way open up new possibilities to understand complex human brain functions, e.g., related to decision-making or emotions.

In the StudyForrest data, we found brain regions with relatively low mean ISCs but relatively high variability of ISCs (see Figs. 3(B), 4(B) and 4(D)). This indicates similar brain processing across some of the subjects but not the majority of them. Interestingly, these clusters were spatially contiguous and located in meaningful cortical brain areas, suggesting that the revealed clusters did characterize brain-activity-related information instead of noise. The fact that many clusters were bilaterally symmetric also supports this view. Yet another indication of brain-activity-related processing in these regions is high variability in ISCs, because it means that there must be both high (positive and/or negative) and low (close to zero) pairwise correlation values present. Noise would be rather reflected by both low mean and low variability in ISCs, which is the case when most pairwise ISC values are close to zero. Our findings are supported

bioRxiv preprint doi: https://doi.org/10.1101/057620; this version posted June 7, 2016. The copyright holder for this preprint (which was not certified by peer review) is the author/funder, who has granted bioRxiv a license to display the preprint in perpetuity. It is made available under aCC-BY-NC-ND 4.0 International license.

by recent functional connectivity studies which indicate that functional/spatial variability in the brain connectivity between individuals characterizes meaningful information [39, 38, 13, 16, 15].

Clusters characterized by low mean ISC but high variability were mainly found in the StudyForrest data set and not in the ICBM data set (see Fig. 4). Moreover, FuSeISC revealed brain areas in the StudyForrest data that were not detected by a conventional ISC analysis (see Fig. 2). These facts and spatial locations of the found clusters in the StudyForrest data set suggest that FuSeISC is capable of characterizing brain areas involved in higher-order processing.

### *5.3. Methodological considerations*

Although many cluster analysis techniques have been previously proposed for the functional segmentation of the human brain from fMRI data [40, 41, 42, 43, 44, 45], they have certain limitations when analyzing complex group fMRI data collected under diverse stimuli. Our method was particularly designed to address some of the key problems. For instance, conventional functional segmentation methods construct group-level segmentations by averaging results across individual subjects, ignoring inherent variability in brain functions across subjects. FuSeISC inherently constructs group-level ISC maps using statistical information of the ISC and this way accounts both for similarity and variability in hemodynamic responses across subjects.

Recently, a group-level model-based cluster analysis framework has been presented that accounts for inter-subject variability [46, 27]. However, this approach requires the model of the experimental paradigm and is therefore not applicable for fMRI data sets collected under naturalistic stimuli. [47] constructed functional segmentations separately for individuals using an iterative algorithm starting from the solution of the population atlas. While this approach takes individual differences into account, visual inspection of brain maps for each individual separately is a tedious task and makes large-scale neuroscientific analysis difficult. FuSeISC integrates data across all subjects and time-series of interest into a single brain map and this way summarizes heterogeneous data into a

bioRxiv preprint doi: https://doi.org/10.1101/057620; this version posted June 7, 2016. The copyright holder for this preprint (which was not certified by peer review) is the author/funder, who has granted bioRxiv a license to display the preprint in perpetuity. It is made available under aCC-BY-NC-ND 4.0 International license.

meaningful amount of information for visual inspection.

Many existing functional segmentation methods constrain segmentation into spatially local neighborhood (see e.g. [45, 41]). FuSeISC does not assume that the clusters are spatially connected, but it is completely data-driven in this sense; the voxels are clustered without any knowledge about their spatial location. This is plausible from neuroscientific perspective, as it allows for the detection of spatially distributed clusters as well as clusters with heavily different sizes. Moreover, since spatial information is not used in the clustering process itself, visual inspection of the spatial locations of the clusters as well as spatial compactness of the clusters serves as a useful validation of the clustering outcome. We found spatially compact clusters from the fMRI data sets in our analyses (differently colored areas in Fig. 3), indicating that the obtained segmentations reflect inherent structures of the data sets and not noise.

Another great benefit of the FuseISC is that it is a non-parametric method in the sense that no ad hoc parameters need to be selected to perform functional segmentation. The method contains one user definable parameter $k$ which controls the coarseness of segmentation, but we proposed a selection of this parameter based on stability plots of the segmentations (see Figs. 5 and 6(B-C)). Technically, $k$ is used to decide the number of neighbors in $k$-NN lists and the subsequent optimally sparsified SNN graph. The graph, in turn, was used as a basis to initialize the GMM to improve its estimation accuracy. This way, $k$ is only indirectly related the number of clusters that the clustering algorithm produces. Based on our simulations with synthetic data, the value of $k$ can be approximately interpreted as the number of voxels that each cluster should minimally contain (see Section 4 in supplementary material). Due to complexity of fMRI data, we proposed a systematic way to choose $k$ based on the stability analysis of the number of clusters and similarity of the segmentation solutions. For the tested data sets, the number of clusters stabilized close to 20 (irrespective of the dataset) and these main clusters were analyzed in this work. Interestingly, the number of found clusters approximately coincides with the number of functional networks used in a recent study in which individual-level

bioRxiv preprint doi: https://doi.org/10.1101/057620; this version posted June 7, 2016. The copyright holder for this preprint (which was not certified by peer review) is the author/funder, who has granted bioRxiv a license to display the preprint in perpetuity. It is made available under aCC-BY-NC-ND 4.0 International license.

functional parcellations were constructed [47]. A population atlas used in that study was constructed in a previous study [48] and involved 18 networks.

The usage of smaller $k$ values resulted in more functional segments as illustrated in Fig. 5(A). For more detailed parcellations, a smaller $k$ could be used. The smaller $k$ values can be useful also to investigate some dedicated region of interest, either defined based on neuroanatomy or by a more coarse functional segmentation.

Due to complex structure of the fMRI data, it is difficult to build an appropriate functional segmentation model in a general case. To alleviate the particular problems associated with the learning of the cluster model and selection of the number of clusters, we proposed a new method based on SNN graph construction to initialize the GMM (see Appendix A.1). The method was successfully validated against the well-known methods $K$-means [30], $K$-means++ [31], Farthest first traversal algorithm [49, 50], Affinity propagation [32], and Ward's minimum variance method [29] using simulated data sets containing Gaussian clusters and outliers (see Section 3 in supplementary material). These techniques were selected as they have been previously reported as useful in the initialization of the GMM, see for instance [51, 52, 25, 53]. Moreover, all these methods can be conveniently controlled with a single user parameter, making them well-comparable against the proposed method. Although derived from a different point of view, we found a very close correspondence in the clustering quality between our method and AP. This was a surprising finding which deserves further investigation in future. In any case, the benefit of our method over AP (as well as Ward's minimum variance method) is that the full distance matrix needs not to be saved in the memory, allowing a large-scale segmentation across the whole-brain without the need for imposing any spatial constraints for the clustering process.

Although FuSeISC is geared towards naturalistic stimulation studies, nothing prevents its application to traditional fMRI studies with strictly controlled stimulus. The application of FuSeISC to these kinds of studies is partially supported by the finding that within these setups activations detected by ISC

bioRxiv preprint doi: https://doi.org/10.1101/057620; this version posted June 7, 2016. The copyright holder for this preprint (which was not certified by peer review) is the author/funder, who has granted bioRxiv a license to display the preprint in perpetuity. It is made available under aCC-BY-NC-ND 4.0 International license.

match well with those detected by the standard GLM analysis [9, 20]. However, it should be noted that the ISC method expects that the subjects experience the same stimulus and therefore, FuSeISC is not useful to segment resting-state fMRI data as done for example by using group-ICA [54, 55].

### *5.4. Applications*

In addition to being a tool for the spatial exploration of large fMRI datasets obtained using naturalistic stimuli (such as the StudyForrest data [17] in this work), FuSeISC has other potential applications. For example, FuSeISC could be used to generate a functional atlas, either from a certain region of interest or from the whole brain, based on task-related fMRI by choosing functionally specific time series for the analysis. This approach would be rather different than constructing atlases based on resting-state fMRI (see [41] and references therein) as one needs to constrain the brain functions to be represented by the atlas. As can be seen in Fig. 3, to achieve a resolution level of the currently commonly used resting-state fMRI atlases, a whole brain atlas would require larger and more diverse datasets than the ones applied in this work. However, combined with a high-resolution fMRI of naturalistic experiments, our approach represents an interesting line for future research. In principle, FuSeISC is not sensitive to the type of the stimulus, meaning that block-design, event-related, and naturalistic experiments could be combined together (at least when fMRI of the same set of subjects is acquired using the same scanner), partly facilitating atlas construction. Studying to what extent data combination is possible in practice is left for future research.

Also, as demonstrated in Fig. 4, FuSeISC provides specific information about the ISC statistics of the time series of interest for each cluster, which can be used to trace clusters back to stimulus features. The prerequisite is that the time series were selected intelligibly so that the whole time series is meaningful for the interpretation. However, in combination with naturalistic stimulation, rich annotations of the stimulus sequence can be used to divide the data into meaningful time series that can then be analysed using FuSeISC.

bioRxiv preprint doi: https://doi.org/10.1101/057620; this version posted June 7, 2016. The copyright holder for this preprint (which was not certified by peer review) is the author/funder, who has granted bioRxiv a license to display the preprint in perpetuity. It is made available under aCC-BY-NC-ND 4.0 International license.

## 6. Conclusions

We have proposed a new data-driven method called FuSeISC to analyze fMRI data sets collected from a group of subjects experiencing variety of stimulus. Unlike conventional ISC analysis, FuSeISC segregates different brain areas based on the ISC statistics of the stimuli of interest and thus segments the human brain into functional segments. FuSeISC performs clustering directly on the basis of individual data of a group of subjects without the requirement for averaging information across subjects, making it rather different from conventional functional segmentation algorithms designed for the fMRI data sets. In addition to spatial information, FuSeISC provides specific information about the ISC statistics of the time series of interest for each cluster as well as information how the ISC statistics differs between clusters.

bioRxiv preprint doi: https://doi.org/10.1101/057620; this version posted June 7, 2016. The copyright holder for this preprint (which was not certified by peer review) is the author/funder, who has granted bioRxiv a license to display the preprint in perpetuity. It is made available under aCC-BY-NC-ND 4.0 International license.

## Appendix A. Construction of initial Gaussian mixture model

### *Appendix A.1. Generation of candidate models*

Here we describe a simple but efficient technique for restricting a set of initial Gaussian mixture model (GMM) candidates *a priori*. To find good candidate models, we capture intrinsic structure of the data by *shared nearest neighbor* (SNN) graphs [28] (also called mutual nearest neighbor graphs). In the SNN graph, two data points are connected only if they belong to each other's $k$-nearest neighbor sets. More formally, let us denote the set of $L$ data points in a $d$-dimensional feature space as $D = \{\mathbf{x}_1, \mathbf{x}_2, ..., \mathbf{x}_L\} \subset \mathbb{R}^d$, and let the set of the $k$-nearest neighbors[9] of an arbitrary data point $\mathbf{x}_m$ be $N_m$. In the SNN graph $G(D, E)$, the vertex set $D$ contains all the data points and the edge set $E$ is given as follows [28]:

$$E = \left\{ (\mathbf{x}_m, \mathbf{x}_n) \left| \mathbf{x}_m \in N_n \wedge \mathbf{x}_n \in N_m \right. \right\}. \tag{A.1}$$

Furthermore, we weight every edge in $E$ of the SNN graph by counting the total number of intersecting data points of the two nearest neighbor sets:

$$w(\mathbf{x}_m, \mathbf{x}_n) = |N_n \cap N_m|. \tag{A.2}$$

Note that by using this weighting scheme, the similarity between two connected data points does not depend on their *absolute distance* but the similarity between data points is determined by the *similarity of the $k$-nearest neighbor sets of these data points*. This desirable property allows detection of clusters with varying densities even in a high-dimensional feature space [56, 57, 58]. We also compute a *degree* for each data point $\mathbf{x}_m$ as the sum of the weights of edges connecting $\mathbf{x}_m$ and its nearest neighbors:

$$deg(\mathbf{x}_m) = \sum_{\mathbf{x}_n \in \mathrm{N}_m} w(\mathbf{x}_m, \mathbf{x}_n). \tag{A.3}$$

[9] A point is not its own neighbor, i.e. $\mathbf{x}_m \notin N_m$.

bioRxiv preprint doi: https://doi.org/10.1101/057620; this version posted June 7, 2016. The copyright holder for this preprint (which was not certified by peer review) is the author/funder, who has granted bioRxiv a license to display the preprint in perpetuity. It is made available under aCC-BY-NC-ND 4.0 International license.

Next, we form multiple candidate (sub)graphs through *sparsification* of the weighted SNN graph. More specifically, to form a single candidate, we remove all the edges associated with data points $\mathbf{x}_m$ whose degree values are below a selected threshold $T_j$. Several candidates are formed using multiple thresholds $T_j$, for $j = 1, 2, \ldots, q$.[10] Thus, a final set of candidate graphs is:

$$A_{\tilde{G}} = \left\{ \tilde{G}_1 \left( D, \tilde{E}_1 \right), \ \tilde{G}_2 \left( D, \tilde{E}_2 \right), ..., \tilde{G}_q \left( D, \tilde{E}_q \right) \right\},$$

where the edge sets of the candidate graphs are:

$$\tilde{E}_j = \left\{ (\mathbf{x}_m, \mathbf{x}_n) \in E \middle| deg\left(\mathbf{x}_m\right), deg\left(\mathbf{x}_n\right) \geq T_j \right\}, \tag{A.4}$$

for $j = 1, 2, \ldots, q$. Finally, we locate the centers of the connected components in each candidate graph:

$$\tilde{\boldsymbol{\mu}}_{i,j} = \mathbf{f}\left(P_{i,j}\right), \tag{A.5}$$

for $i = 1, 2, ..., h_j$. In this expression, $\tilde{\boldsymbol{\mu}}_{i,j}$ denotes the center of the $i$th connected component in the $j$th graph $\tilde{G}_j$, the set $P_{i,j}$ contains all the data points associated with that component, and $h_j$ is the total number of connected components in that graph. The function $\mathbf{f}(\cdot)$ summarizes the connected component in a meaningful way. Our default choice for $\mathbf{f}(\cdot)$ is the mean of the data points of the $P_{i,j}$.

### *Appendix A.2. Choice of initial GMM*

Given the candidate sets $C_1$, $C_2$, ..., $C_q$ of the mean vectors, the next task is to choose one set $C_j = \left\{ \tilde{\boldsymbol{\mu}}_{1,j}, \tilde{\boldsymbol{\mu}}_{2,j}, ..., \tilde{\boldsymbol{\mu}}_{h_j,j} \right\}$ that represents all clusters in data. Different criteria can be used for this purpose, including well-known Bayesian information criterion (BIC) [59] or simple minimum sum-of-squared error (SSE) criterion (minimum distance rule). In our tests with synthetic noisy

[10] A most systematic approach is to construct as many candidates as there are distinct degree values. Note that degree values are integers and the maximum possible value is $k(k-1)$. Therefore, the number of distinct candidate graphs is $q \leq k(k-1)$).

bioRxiv preprint doi: https://doi.org/10.1101/057620; this version posted June 7, 2016. The copyright holder for this preprint (which was not certified by peer review) is the author/funder, who has granted bioRxiv a license to display the preprint in perpetuity. It is made available under aCC-BY-NC-ND 4.0 International license.

fMRI data, we found slightly more stable clustering results with the SSE than BIC (see Section 5 in supplementary material) and therefore we used SSE as the criterion in this paper.[11]

After selecting the best candidate set of mean vectors, we use a minimum distance rule to assign data points to clusters, and estimate corresponding covariance matrices. The obtained mean vectors and covariance matrices form our initial GMM.

*Author Contributions*

Conceived and designed the experiments: JPK, JP, JT. Performed the experiments: JPK, JP. Analyzed the data: JPK,RH,JT. Wrote the paper: JPK, JP, RH, JT. Contributed new clustering algorithm: JPK, JN.

*Acknowledgments*

JPK was funded by the Academy of Finland Postdoctoral Researcher program (Research Council for Natural Sciences and Engineering; grant number 286019).

JT received funding from the Universidad Carlos III de Madrid, the European Union's Seventh Framework Programme for research, technological development and demonstration under grant agreement nr 600371, el Ministerio de Economía y Competitividad (COFUND2013-40258) and Banco Santander.

Data collection and sharing for this project were provided in part by the International Consortium for Brain Mapping (ICBM; Principal Investigator: John Mazziotta, M.D., Ph.D.). ICBM funding was provided by the National Institute of Biomedical Imaging and BioEngineering. ICBM data are disseminated by the Laboratory of Neuro Imaging at the University of Southern California.

*Conflicting interests*

The authors declare no conflicting interests.

[11] We found out that SSE criterion returns meaningful solutions in which all clusters are represented by estimated centroids $\tilde{\boldsymbol{\mu}}$ and these solutions did not always coincide with the most complex model in the formed candidate sets. This can be explained by varying locations of estimated centroids between different candidate models.

bioRxiv preprint doi: https://doi.org/10.1101/057620; this version posted June 7, 2016. The copyright holder for this preprint (which was not certified by peer review) is the author/funder, who has granted bioRxiv a license to display the preprint in perpetuity. It is made available under aCC-BY-NC-ND 4.0 International license.

## References

[1] U. Hasson, Y. Nir, I. Levy, G. Fuhrmann, R. Malach, Intersubject synchronization of cortical activity during natural vision, Science 303 (2004) 1634–1640.

[2] Y. Golland, S. Bentin, H. Gelbard, Y. Benjamini, R. Heller, Y. Nir, U. Hasson, R. Malach, Extrinsic and intrinsic systems in the posterior cortex of the human brain revealed during natural sensory stimulation, Cerebral Cortex 17 (2007) 766–777.

[3] L. Nummenmaa, E. Glerean, M. Viinikainen, I. P. Jääskeläinen, R. Hari, M. Sams, Emotions promote social interaction by synchronizing brain activity across individuals, Proceedings of the National Academy of Sciences 109 (2012) 9599–9604.

[4] M. Reason, C. Jola, R. Kay, D. Reynolds, J.-P. Kauppi, M.-H. Grobras, J. Tohka, F. E. Pollick, Spectators' aesthetic experience of sound and movement in dance performance: A transdisciplinary investigation., Psychology of Aesthetics, Creativity, and the Arts 10 (2016) 42.

[5] W. Trost, S. Frühholz, T. Cochrane, Y. Cojan, P. Vuilleumier, Temporal dynamics of musical emotions examined through intersubject synchrony of brain activity, Social cognitive and affective neuroscience 10 (2015) 1705–1721.

[6] D. A. Abrams, S. Ryali, T. Chen, P. Chordia, A. Khouzam, D. J. Levitin, V. Menon, Inter-subject synchronization of brain responses during natural music listening, European Journal of Neuroscience 37 (2013) 1458–1469.

[7] S. M. Wilson, I. Molnar-Szakacs, M. Iacoboni, Beyond superior temporal cortex: Intersubject correlations in narrative speech comprehension, Cerebral Cortex 18 (2008) 230–242.

bioRxiv preprint doi: https://doi.org/10.1101/057620; this version posted June 7, 2016. The copyright holder for this preprint (which was not certified by peer review) is the author/funder, who has granted bioRxiv a license to display the preprint in perpetuity. It is made available under aCC-BY-NC-ND 4.0 International license.

[8] J.-P. Kauppi, I. P. Jääskeläinen, M. Sams, J. Tohka, Inter-subject correlation of brain hemodynamic responses during watching a movie: localization in space and frequency, Frontiers in Neuroinformatics 4 (2010) 5.

[9] J. Pajula, J.-P. Kauppi, J. Tohka, Inter-subject correlation in fMRI: method validation against stimulus-model based analysis, PLOS ONE 7 (2012) e41196.

[10] K. J. Friston, A. P. Holmes, K. J. Worsley, J.-P. Poline, C. D. Frith, R. S. Frackowiak, Statistical parametric maps in functional imaging: a general linear approach, Human brain mapping 2 (1994) 189–210.

[11] U. Hasson, R. Malach, D. J. Heeger, Reliability of cortical activity during natural stimulation, Trends in cognitive sciences 14 (2010) 40–48.

[12] J. Kauppi, I. Jaaskelainen, M. Sams, J. Tohka, Clustering inter-subject correlation matrices in functional magnetic resonance imaging, in: Information Technology and Applications in Biomedicine (ITAB), 2010 10th IEEE International Conference on, IEEE, pp. 1–6.

[13] S. Mueller, D. Wang, M. D. Fox, B. Yeo, J. Sepulcre, M. R. Sabuncu, R. Shafee, J. Lu, H. Liu, Individual variability in functional connectivity architecture of the human brain, Neuron 77 (2012) 586–595.

[14] K. Zilles, K. Amunts, Individual variability is not noise, Trends in Cognitive Sciences 17 (2013) 153 – 155.

[15] R. Boldt, M. Seppä, S. Malinen, P. Tikka, R. Hari, S. Carlson, Spatial variability of functional brain networks in early-blind and sighted subjects, NeuroImage 95 (2014) 208–216.

[16] S. Gopal, R. L. Miller, S. A. Baum, V. D. Calhoun, Approaches to capture variance differences in rest fmri networks in the spatial geometric features: Application to schizophrenia, Frontiers in Neuroscience 10 (2016).

bioRxiv preprint doi: https://doi.org/10.1101/057620; this version posted June 7, 2016. The copyright holder for this preprint (which was not certified by peer review) is the author/funder, who has granted bioRxiv a license to display the preprint in perpetuity. It is made available under aCC-BY-NC-ND 4.0 International license.

[17] M. Hanke, F. J. Baumgartner, P. Ibe, F. R. Kaule, S. Pollmann, O. Speck, W. Zinke, J. Stadler, A high-resolution 7-Tesla fMRI dataset from complex natural stimulation with an audio movie, Scientific Data 1 (2014).

[18] J.-P. Kauppi, J. Pajula, J. Tohka, A Versatile software package for inter-subject correlation based analyses of fMRI, Frontiers in Neuroinformatics 8 (2014).

[19] J. Mazziotta, A. Toga, A. Evans, P. Fox, J. Lancaster, K. Zilles, R. Woods, T. Paus, G. Simpson, B. Pike, C. Holmes, L. Collins, P. Thompson, D. MacDonald, M. Iacoboni, T. Schormann, K. Amunts, N. Palomero-Gallagher, S. Geyer, L. Parsons, K. Narr, N. Kabani, G. L. Goualher, D. Boomsma, T. Cannon, R. Kawashima, B. Mazoyer, A probabilistic atlas and reference system for the human brain: International consortium for brain mapping (icbm), Philosophical Transactions of the Royal Society of London.Series B: Biological Sciences 356 (2001) 1293–1322.

[20] J. Pajula, J. Tohka, Effects of spatial smoothing on inter-subject correlation based analysis of fMRI, Magnetic resonance imaging 32 (2014) 1114–1124.

[21] J. Smith, Spectral Audio Signal Processing, http://ccrma.stanford.edu/~jos/sasp/, Accessed 02.05.2012. Online book.

[22] M. Van Den Heuvel, R. Mandl, H. Hulshoff Pol, Normalized cut group clustering of resting-state fMRI data, PloS one 3 (2008) e2001.

[23] G. McLachlan, D. Peel, Finite Mixture Models (Wiley Series in Probability and Statistics), Wiley-Interscience, 1 edition, 2000.

[24] L. Xu, M. I. Jordan, On convergence properties of the em algorithm for gaussian mixtures, Neural computation 8 (1996) 129–151.

[25] C. Fraley, A. E. Raftery, Model-based clustering, discriminant analysis, and density estimation, Journal of the American statistical Association 97 (2002) 611–631.

bioRxiv preprint doi: https://doi.org/10.1101/057620; this version posted June 7, 2016. The copyright holder for this preprint (which was not certified by peer review) is the author/funder, who has granted bioRxiv a license to display the preprint in perpetuity. It is made available under aCC-BY-NC-ND 4.0 International license.

[26] M. A. F. Figueiredo, A. K. Jain, Unsupervised learning of finite mixture models, IEEE Trans. Pattern. Anal. Mach. Intell. 24 (2002) 381–396.

[27] B. Thirion, G. Varoquaux, E. Dohmatob, J.-B. Poline, Which fMRI clustering gives good brain parcellations?, Frontiers in Neuroscience 8 (2014).

[28] R. A. Jarvis, E. A. Patrick, Clustering using a similarity measure based on shared near neighbors, IEEE Trans. on Computers 100 (1973) 1025–1034.

[29] J. Ward, Hierarchical Grouping to Optimize an Objective Function, J. Am. Stat. Ass. 58 (1963) 236–244.

[30] J. B. Macqueen, Some methods of classification and analysis of multivariate observations, in: Proc. of the 5th Berkeley Symp. on Math. Stat. and Probability, pp. 281–297.

[31] D. Arthur, S. Vassilvitskii, k-means++: the advantages of careful seeding, in: SODA '07: Proceedings of the eighteenth annual ACM-SIAM symposium on Discrete algorithms, Society for Industrial and Applied Mathematics, Philadelphia, PA, USA, 2007, pp. 1027–1035.

[32] B. Frey, D. Dueck, Clustering by Passing Messages Between Data Points, Science 315 (2007) 972–976.

[33] S. Pamilo, S. Malinen, Y. Hlushchuk, M. Seppä, P. Tikka, R. Hari, Functional subdivision of group-ICA results of fMRI data collected during cinema viewing, PloS one 7 (2012) e42000.

[34] R. Boldt, S. Malinen, M. Seppä, P. Tikka, P. Savolainen, R. Hari, S. Carlson, Listening to an audio drama activates two processing networks, one for all sounds, another exclusively for speech, PloS one 8 (2013) e64489.

[35] K. J. Gorgolewski, G. Varoquaux, G. Rivera, Y. Schwartz, V. V. Sochat, S. S. Ghosh, C. Maumet, T. E. Nichols, J.-B. Poline, T. Yarkoni, D. S. Margulies, R. A. Poldrack, Neurovault.org: A repository for sharing unthresholded statistical maps, parcellations, and atlases of the human brain, NeuroImage (2015). Available online 11 April 2015.

bioRxiv preprint doi: https://doi.org/10.1101/057620; this version posted June 7, 2016. The copyright holder for this preprint (which was not certified by peer review) is the author/funder, who has granted bioRxiv a license to display the preprint in perpetuity. It is made available under aCC-BY-NC-ND 4.0 International license.

[36] S. Malinen, Y. Hlushchuk, R. Hari, Towards natural stimulation in fMRI—issues of data analysis, Neuroimage 35 (2007) 131–139.

[37] C. Speelman, M. McGann, How mean is the mean?, Frontiers in Psychology 4 (2013).

[38] D. Wang, H. Liu, Functional connectivity architecture of the human brain not all the same, The Neuroscientist 20 (2014) 432–438.

[39] D. V. Smith, A. V. Utevsky, A. R. Bland, N. Clement, J. A. Clithero, A. E. Harsch, R. M. Carter, S. A. Huettel, Characterizing individual differences in functional connectivity using dual-regression and seed-based approaches, NeuroImage 95 (2014) 1–12.

[40] C. Goutte, P. Toft, E. Rostrup, F. Å. Nielsen, L. K. Hansen, On clustering fMRI time series, NeuroImage 9 (1999) 298–310.

[41] R. C. Craddock, G. James, P. E. Holtzheimer, X. P. Hu, H. S. Mayberg, A whole brain fMRI atlas generated via spatially constrained spectral clustering, Human Brain Mapping 33 (2012) 1914–1928.

[42] M. van den Heuvel, R. Mandl, H. Hulshoff Pol, Normalized cut group clustering of resting-state fmri data, PLoS ONE 3 (2008) e2001.

[43] E. Maggioni, M. G. Tana, F. Arrigoni, C. Zucca, A. M. Bianchi, Constructing fMRI connectivity networks: a whole brain functional parcellation method for node definition, Journal of neuroscience methods 228 (2014) 86–99.

[44] P. Bellec, P. Rosa-Neto, O. C. Lyttelton, H. Benali, A. C. Evans, Multi-level bootstrap analysis of stable clusters in resting-state fMRI, Neuroimage 51 (2010) 1126–1139.

[45] T. Blumensath, S. Jbabdi, M. F. Glasser, D. C. Van Essen, K. Ugurbil, T. E. Behrens, S. M. Smith, Spatially constrained hierarchical parcellation of the brain with resting-state fMRI, Neuroimage 76 (2013) 313–324.

bioRxiv preprint doi: https://doi.org/10.1101/057620; this version posted June 7, 2016. The copyright holder for this preprint (which was not certified by peer review) is the author/funder, who has granted bioRxiv a license to display the preprint in perpetuity. It is made available under aCC-BY-NC-ND 4.0 International license.

[46] D. Lashkari, R. Sridharan, E. Vul, P.-J. Hsieh, N. Kanwisher, P. Golland, Search for patterns of functional specificity in the brain: a nonparametric hierarchical Bayesian model for group fMRI data, Neuroimage 59 (2012) 1348–1368.

[47] D. Wang, R. L. Buckner, M. D. Fox, D. J. Holt, A. J. Holmes, S. Stoecklein, G. Langs, R. Pan, T. Qian, K. Li, et al., Parcellating cortical functional networks in individuals, Nature neuroscience (2015).

[48] B. T. Yeo, F. M. Krienen, J. Sepulcre, M. R. Sabuncu, D. Lashkari, M. Hollinshead, J. L. Roffman, J. W. Smoller, L. Zöllei, J. R. Polimeni, et al., The organization of the human cerebral cortex estimated by intrinsic functional connectivity, Journal of neurophysiology 106 (2011) 1125–1165.

[49] D. S. Hochbaum, D. B. Shmoys, A Best Possible Heuristic for the k-Center Problem, Mathematics of Operations Research 10 (1985) 180–184.

[50] T. Gonzalez, Clustering to minimize the maximum intercluster distance, Theor. Comp. Sci. 38 (1985) 293–306.

[51] D. Dueck, Affinity Propagation: Clustering data by passing messages, Ph.D. thesis, University of Toronto, 2009.

[52] S. Dasgupta, L. J. Schulman, A two-round variant of EM for Gaussian mixtures, in: Proc. of 16th conf. on Uncert. in Artif. Intell., Morgan Kaufmann Publishers Inc., pp. 152–159.

[53] J. Blömer, K. Bujna, Simple methods for initializing the EM algorithm for Gaussian mixture models, arXiv preprint arXiv:1312.5946 (2013).

[54] V. Kiviniemi, T. Starck, J. Remes, X. Long, J. Nikkinen, M. Haapea, J. Veijola, I. Moilanen, M. Isohanni, Y.-F. Zang, et al., Functional segmentation of the brain cortex using high model order group PICA, Human brain mapping 30 (2009) 3865–3886.

bioRxiv preprint doi: https://doi.org/10.1101/057620; this version posted June 7, 2016. The copyright holder for this preprint (which was not certified by peer review) is the author/funder, who has granted bioRxiv a license to display the preprint in perpetuity. It is made available under aCC-BY-NC-ND 4.0 International license.

[55] C. F. Beckmann, M. DeLuca, J. T. Devlin, S. M. Smith, Investigations into resting-state connectivity using independent component analysis, Philosophical Transactions of the Royal Society of London B: Biological Sciences 360 (2005) 1001–1013.

[56] P. Tan, M. Steinbach, V. Kumar, Introduction to Data Mining, Addison-Wesley, 2014.

[57] L. Ertöz, M. Steinbach, V. Kumar, Finding clusters of different sizes, shapes, and densities in noisy, high dimensional data, in: in Proc. of 2nd SIAM Int. Conf. on Data Mining.

[58] M. Houle, H.-P. Kriegel, P. Kröger, E. Schubert, A. Zimek, Can Shared-Neighbor Distances Defeat the Curse of Dimensionality?, in: M. Gertz, B. Ludäscher (Eds.), Scientific and Statistical Database Management, volume 6187 of *Lecture Notes in Computer Science*, Springer Berlin / Heidelberg, Berlin, Heidelberg, 2010, pp. 482–500.

[59] G. Schwarz, et al., Estimating the dimension of a model, The annals of statistics 6 (1978) 461–464.